Cancer Research

BRG1/SMARCA4 Inactivation Promotes Non–Small Cell Lung Cancer Aggressiveness by Altering Chromatin Organization

Tess Orvis[1], Austin Hepperla[1,2], Vonn Walter[1], Shujie Song[1,3], Jeremy Simon[1,4], Joel Parker[1,5], Matthew D. Wilkerson[1,5], Nisarg Desai[1], Michael B. Major[1,6], D. Neil Hayes[1,7], Ian J. Davis[1,5,8], and Bernard Weissman[1,9]

Abstract

SWI/SNF chromatin remodeling complexes regulate critical cellular processes, including cell-cycle control, programmed cell death, differentiation, genomic instability, and DNA repair. Inactivation of this class of chromatin remodeling complex has been associated with a variety of malignancies, including lung, ovarian, renal, liver, and pediatric cancers. In particular, approximately 10% of primary human lung non–small cell lung cancers (NSCLC) display attenuations in the BRG1 ATPase, a core factor in SWI/SNF complexes. To evaluate the role of BRG1 attenuation in NSCLC development, we examined the effect of BRG1 silencing in primary and established human NSCLC cells. BRG1 loss altered cellular morphology and increased tumorigenic potential. Gene expression analyses showed reduced expression of genes known to be associated with progression of human NSCLC. We demonstrated that BRG1 losses in NSCLC cells were associated with variations in chromatin structure, including differences in nucleosome positioning and occupancy surrounding transcriptional start sites of disease-relevant genes. Our results offer direct evidence that BRG1 attenuation contributes to NSCLC aggressiveness by altering nucleosome positioning at a wide range of genes, including key cancer-associated genes. *Cancer Res; 74(22); 6486–98. ©2014 AACR.*

Introduction

Studies of the molecular mechanisms of non–small cell lung cancer (NSCLC) development have identified alterations in oncogene expression and inactivation of tumor suppressor genes, including *ALK*, *KRAS*, *EGFR*, *RB*, $p16^{INK4A}$, and *p53* (1, 2). Recently, loss of BRG1 expression through mutations or other mechanisms has been observed in 10% of NSCLCs (3–7). The *BRG1* gene, also known as *SMARCA4*, encodes one of the two mutually exclusive ATPase subunits of the SWI/SNF chromatin remodeling complex. The SWI/SNF complex, first discovered in *saccharomyces cerevisiae*, acts as a positive regulator of the HO endonuclease and Suc2 genes (8–10). The complexes contain approximately 10 to 12 components that show strong conservation of protein structure and function from yeast to *Drosophila* to mammals (11, 12). Mutations in members of the complex have been found in human cancers, including NSCLC, malignant rhabdoid tumors, ovarian carcinomas, and renal cell carcinomas, suggesting that loss of chromatin maintenance through active nucleosome positioning is associated with cancer development (3–7, 13, 14). How *BRG1* inactivation contributes to the development of NSCLC remains unresolved.

In a previous study, we demonstrated that induction of BRG1 in BRG1-deficient tumor cell lines leads to reexpression of genes epigenetically silenced during NSCLC development (15, 16). Intriguingly, the genes reactivated after BRG1 reexpression did not seem to undergo changes in promoter methylation (15). These results suggested that BRG1 loss may provide an alternative mechanism for silencing of genes detrimental to the initiation and/or progression of NSCLC. In this current study, we examined the biologic, transcriptional, and chromatin effects of knockdown of BRG1 in NSCLC cell lines. We observed a significant increase in tumorigenic potential upon loss of BRG1 expression in NSCLC cells. We also identified a set of genes with reduced expression upon inactivation of BRG1 by RNAi. We further showed that several of these genes, previously implicated in the etiology of NSCLC, display reduced expression in BRG1-deficient primary NSCLC

[1]Lineberger Comprehensive Cancer Center, University of North Carolina at Chapel Hill, Chapel Hill, North Carolina. [2]Curriculum in Genetics and Molecular Biology, University of North Carolina at Chapel Hill, Chapel Hill, North Carolina. [3]Cancer Center, Zhujiang Hospital, Southern Medical University, Guangzhou, Guangdong, P.R. China. [4]Curriculum in Bioinformatics and Computational Biology, University of North Carolina at Chapel Hill, Chapel Hill, North Carolina. [5]Department of Genetics, University of North Carolina at Chapel Hill, Chapel Hill, North Carolina. [6]Department of Cell Biology and Physiology, University of North Carolina, Chapel Hill, North Carolina. [7]Department of Medicine, University of North Carolina at Chapel Hill, Chapel Hill, North Carolina. [8]Department of Pediatrics and Carolina Center for Genome Sciences, University of North Carolina at Chapel Hill, Chapel Hill, North Carolina. [9]Department of Pathology and Laboratory Medicine, University of North Carolina at Chapel Hill, Chapel Hill, North Carolina.

Note: Supplementary data for this article are available at Cancer Research Online (http://cancerres.aacrjournals.org/).

T. Orvis, A. Hepperla, and V. Walter contributed equally to this article.

I.J. Davis and B. Weissman contributed equally to this article.

Corresponding Authors: Bernard E. Weissman, University of North Carolina, LCCC 32-048, 450 West Drive, Chapel Hill, NC 27599. Phone: 919-966-7533; Fax: 1-919-966-3015; E-mail: weissman@med.unc.edu; and Ian J. Davis, University of North Carolina, LCCC 21-214, 450 West Drive, Chapel Hill, NC 27599. Phone: 919-966-5360; Fax: 919-966-8212; E-mail: ian_davis@med.unc.edu

doi: 10.1158/0008-5472.CAN-14-0061

samples. Finally, we showed that BRG1 loss results in widespread changes in chromatin organization at regions including transcriptional start sites of these target genes. These results suggest that BRG1 mutations/deletions found in primary NSCLCs can provide an alternative mechanism to alter the expression of cancer-associated genes.

Materials and Methods

Cell culture

The H358, H441, SK-MES, H2170, H727, SW900, H2228, H520 and H1395, H1703, H522, A427, H23, H1299, and A549 human NSCLC carcinoma cell lines were used in this study. All cell lines were obtained from the ATCC and always used from frozen stocks within 3 months of acquisition. All cell lines were cultured at 37°C/5%CO2 in RPMI-1640 supplemented with 10% FBS (Gibco; standard growth medium). H358 and H441 cell lines containing stable BRG1 knockdowns, Brg1i.1, Brg1i.2, and Brg1i.3, were maintained in standard growth medium supplemented with 1 μg/mL puromycin or 0.4 mg/mL neomycin.

Generation of BRG1-deficient cell lines

We used two methods to establish stable knockdown cell lines, lentiviral infection (H358 Brg1i.2 and Brg1i.3) and DNA transfection (H358 Brg1i.1). Lentivirus targeting BRG1 with shRNA was purified from 293FT cells (17). 293FT cells were transfected with one of the MISSION shRNA lentiviral transduction particles [TRCN0000015548 (Brg1i.3) or TRCN0000015549 (Brg1i.2)] using Lipofectamine 2000 (Invitrogen) to generate infectious viral particles. The H358 cell line was then infected in the presence of polybrene for 30 minutes. Twenty-four hours after infection, cells were selected with puromycin at 1 μg/mL. Stably infected clones were harvested, expanded, and screened for BRG1 expression by Western blotting. Clones with the most complete BRG1 silencing were combined to generate pooled cell lines for each respective BRG1 knockdown. Similarly treated control cell lines were also generated (Supplementary Fig. S1A).

The H358 Brg1i.1 and the H358 control cell line, designated Control, were generated using PHTP RNAi expression vectors that target BRG1, or the PHTP empty vector, respectively (18, 19). The H358 cell line was transfected with each vector using FuGene (Roche). After 24 hours, stable clones were selected in puromycin at 1 μg/mL. Over 30 Brg1i.1 and 20 Control puromycin-resistant clones were expanded and isolated for further characterization. Clones were screened for reduced BRG1 expression by Western blotting.

To generate stable knockdown H441 cell lines, we infected cells with either pLKO.1, a nontargeting shRNA control vector (SHC002; Sigma), or the MISSION BRG1 shRNA lentiviral transduction particle (TRCN0000015549) and selected with 1 mg/mL puromycin, as described above for the H358 cells. We designated the BRG1 knockdown cell lines as H441 Brg1i.2 (TRCN0000015549) and the control nontargeting shRNA cell line as H441 Control.

In vivo growth assay

Cells (5×10^7) for each cell line were harvested by trypsinization, rinsed with PBS, and resuspended one-to-one in ice-cold Matrigel (BD Biosciences). Six-week-old *Nu/Nu* female mice were inoculated into the left lung with 40 μL (5×10^6 cells/lung) of cell/Matrigel suspension. Mice were monitored daily for signs of distress and were sacrificed when they exhibited weight loss or difficulty in breathing.

Western blotting

Western blotting was performed as previously described (20). Protein expression was analyzed with the following antibodies: anti-BRG1 G7 (sc-17796; Santa Cruz Biotechnology) and anti–β-actin (A2066; Sigma). Secondary mouse IgG and rabbit IgG antibodies (GE Healthcare) were detected with enhanced chemiluminescence (GE Healthcare).

Quantitative real-time reverse transcription PCR analysis

RNA expression was examined by the qRT-PCR analysis as previously described (20). All genes were normalized to β-actin and quantified using the $2^{-\Delta\Delta Ct}$ statistical method (21). The TaqMan primer and probes sets obtained from Applied Biosystems included BRG1 (Hs00946396_m1), SEM3B (Hs00190328_m1), EHF (Hs00171917_m1), DUSP6 (Hs04329643_s1), IL8 (Hs99999034_m1), SYK (Hs00895377_m1), IFI16 (Hs00194261_m1), BATF (Hs00232390_m1), and β-ACTIN (Hs00357333_g1).

Microarray analyses

Total RNA was extracted from H358 (parental), H358 Control (empty vector), and H358 Brg1i.2 and H358 Brg1i.1 (BRG1 shRNA knockdown) cell lines and submitted to the UNC Lineberger Genomics Core for Agilent microarray analysis. RNA was labeled with Cy5 (experimental H358 Control, H358 Brg1i.1, and H358 Brg1i.2) and Cy3 (control H358) and hybridized to 4 × 44 whole human genome microarrays (Agilent Technologies). The normexp background correction and loess normalization procedures were applied to the probe-level data (22). Expression measurements for each gene were calculated by computing the mean of the normalized intensity values for all probes mapping to that gene, as specified in a gene annotation database. This produced expression values for 19,749 genes. These data are available at GEO (http://www.ncbi.nlm.nih.gov/geo/), under accession number GSE58542.

The SAMR package was used to detect differentially expressed genes by comparing the expression values in each of the two BRG1-deficient cell lines with the expression values in the Control cell line (23). Gene expression values were first standardized within each array. Differential expression was then assessed by finding the smallest value of the tuning parameter delta that produced a median FDR smaller than 0.001. A total of 1,000 permutations were used in each analysis.

NSCLC cell line RNA-seq generation and analysis

Nine NSCLC cell lines with wild-type BRG1 (wtBRG1) expression (H358, SK-MES, H2170, H441, H727, SW900, H2228, H520, and H1395) and 6 cell lines with BRG1 nonsense/truncating mutations (mtBRG1; H1703, H522, A427, H23, H1299, and A549) were grown in standard growth medium. Isolated RNA samples were prepared and libraries created

using TruSeq RNA Sample Preparation Kit v2 (Illumina), which included a poly A selection step. Libraries were pooled at 2 nmol/L concentration, and the samples were then subjected to cBot cluster generation using the TruSeq Rapid PE Cluster Kit (Illumina). The amplified libraries were sequenced using the TruSeq Rapid SBS Kit on the HiSeq 2500 (Illumina). mRNA-seq data were aligned with Mapsplice (24) and genes were quantified with RSEM (25). Gene expression estimates were upper quartile normalized (26). For comparison of target gene expression in wtBRG1 versus mtBRG1, gene expression measurements were computed by replacing all RSEM values identically equal to zero with the smallest nonzero RSEM value and then applying a $\log_2$ transformation. The SAMR package was used to detect genes that were differentially expressed when the BRG1-mutant cell lines were compared with the BRG1 wild-type cell lines (23). Using an FDR threshold of 0.025, a total of 135 genes were downregulated in the BRG1-mutant cell lines (Supplementary Table S2).

To identify an expression matched but unregulated gene set for comparison for each cell line, the mean expression of all 275 downregulated genes was calculated. We then used ranked values of the Pearson correlation coefficient to identify a set of 300 genes that had expression patterns most similar to mean expression values across all cell lines. This set of 300 genes was chosen from among those genes that did not belong to the set of 591 differentially expressed genes. Using a similar procedure, for each of the 275 downregulated genes, we identified a set of 100 nondifferentially expressed genes that had expression patterns most similar to each downregulated gene of interest across all cell lines. This produced a list of 1,484 unique genes that contained all of the 300 genes described above. For sampling purposes, RefSeq genes were selected from this group.

Expression analyses of primary NSCLCs

To determine whether reduced BRG1 protein levels correlated with lower mRNA expression in NSCLC, we obtained RNA-seq–based gene expression data from The Cancer Genome Atlas (TCGA) lung adenocarcinoma project. RNA-seq data were analyzed by first replacing all RSEM values identically equal to zero with the smallest nonzero RSEM value, and then a $\log_2$ transformation was applied (25). Samples with

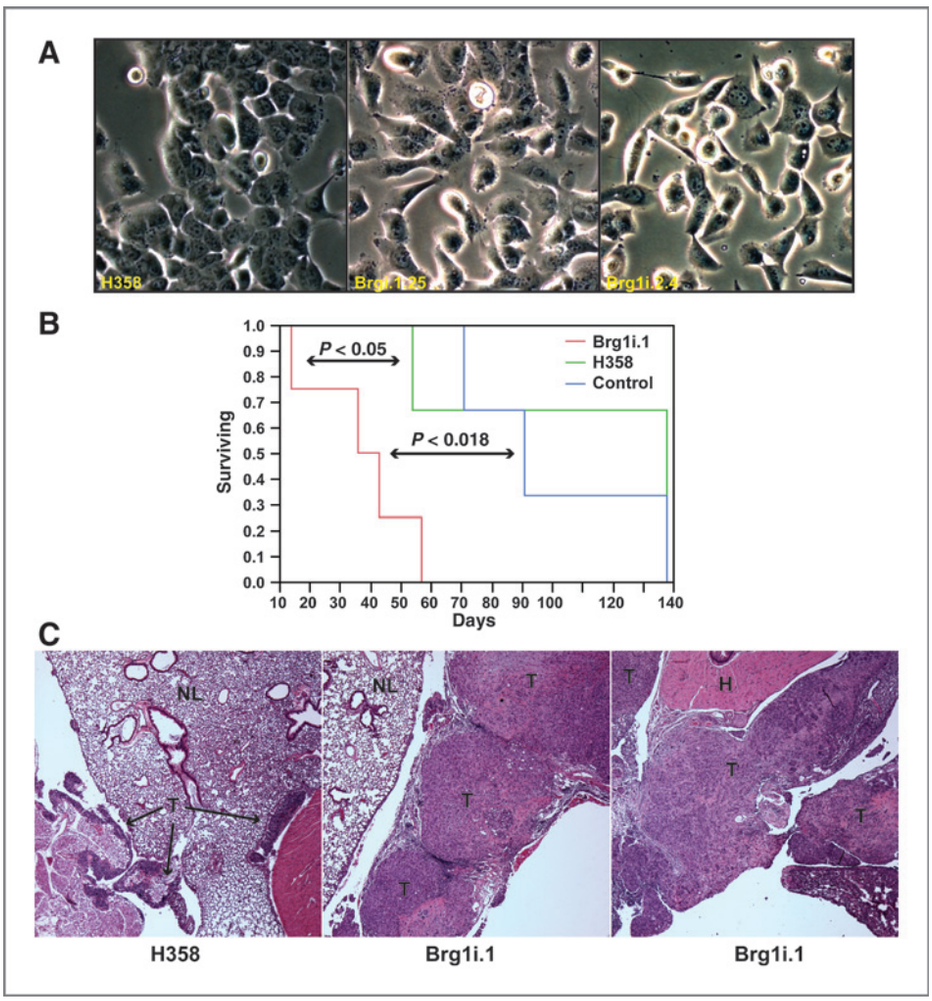

Figure 1. *In vitro* and *in vivo* growth properties of BRG1-deficient H358 cell lines. A, phase contrast photomicrographs of the H358 cell line and clonal cell lines with reduced BRG1 expression (Brg1i.1.25 and Brg1i.2.4). B, each cell line was inoculated intrathoracically into 4 *Nu/Nu* female mice and monitored for tumor development 3× weekly. C, paraffin-embedded sections of representative lung and surrounding tissues from mice after intrathoracic inoculation of parental or Brg1i.1 cells. Mice were sacrificed at 138 days (parental), 36 days (Brg1i.1), and 43 days (Brg1i.1). Sections were stained for histology by hematoxylin and eosin by standard methods (top row). H, heart; NL, normal lung; T, tumor; Magnification, ×400.

BRG1 mutations were identified, and the expression values from samples with nonsense or frame shift mutations were used to identify samples that have reduced *BRG1* expression. The threshold for reduced *BRG1* expression was defined to be the highest *BRG1* expression value observed in any of the samples with *BRG1* nonsense or frameshift mutations. The one-sided Wilcoxon rank sum test was applied to assess the statistical significance of differences in the expression values for specific BRG1 target genes, where the null hypothesis corresponds to no difference in expression and the alternative hypothesis is that expression is lower in samples that have reduced *BRG1* expression, as defined above.

Nuclear extraction and MNase digestion

We initially determined the optimal conditions of MNase digestion to generate a distribution of approximately 35% mononucleosomes for the parental H358 cell line. We then confirmed a similar distribution of nucleosomes after MNase digestion of chromatin for each cell line to preferentially analyze nucleosomes with similar sensitivity to MNase and

Table 1. Genes downregulated in BRG1 knockdown cell lines—differentially expressed genes were identified, as described in Materials and Methods

ABLIM3	C6orf203	EPHA4	HLA-F	LOC728485	PPP1R14C	ST3GAL1
ACSL5	C7orf29	EREG	HLA-H	LOX	PRINS	STAMBPL1
ADAM15	C8orf4	ESPNL	HLA-J	LPXN	PSMB9	STK33
ADFP	C8orf75	F3	HMGA2	LRAT	PTHLH	STXBP6
AGMAT	CA14	FABP6	HNMT	LRMP	PTX3	**SYK**
AHR	CALB2	FAM115C	HPGD	LRRC34	PVRL1	TAOK3
AIM2	CARD16	FAM167A	HS3ST1	MAFF	PXDNL	TAP1
ALDH2	CARD17	FAM176A	HYI	MAGEB2	RAB38	TAPBPL
ALS2CR11	CASP1	FAS	ICAM1	MAOB	RAC2	TBX15
ANGPTL2	CCDC153	FBP1	ICAM2	MAPK13	RAMP1	TFB1M
AN01	CCRL2	FCGR2A	IER3	MARCH1	RBP1	TLR2
ANTXR2	CD163L1	FGF9	**IFI16**	MCTP2	RGS1	TM4SF19
ANXA10	CD52	FGG	IGFBP7	MFI2	RGS2	TMCC3
ANXA2P3	CD63	FLJ23569	IL11	MGC42105	RHBDL2	TMEM117
AP1S2	CFP	FLJ31356	IL15RA	MGP	S100A6	TMEM154
AP3M2	CHODL	FLJ45422	IL1B	MICB	SCG5	TMEM171
AP0BEC3G	CLCA3	FOLR1	IL1RAPL1	MMP7	SDC2	TMEM204
AP0L3	CLCF1	FUT1	IL20RB	MYL5	**SEMA3B**	TMEM22
AREG	CLDND1	GCAT	IL23A	NAP1L3	SEMA7A	TMPRSS13
ARHGAP30	CLIC2	GCHFR	IL28A	NCALD	SERPINB2	TNFAIP8
ARL16	COL7A1	GIMAP2	INHBA	NCRNA0008	SERPINB5	TNFRSF10C
ARRDC4	COR06	GJB5	INPP1	ND2	SERPINB7	TNFRSF14
ATG9A	CPM	GMFG	IRF6	NFKBIZ	SERPINB8	TNFRSF9
AZGP1	CPS1	GPM6A	ITGA7	NOSTRIN	SERPINE2	TPK1
BAK1	CPXCR1	GPR158	ITPR1	NRIP3	SERPINH1	TREM1
BATF	CSF2RA	GPR68	KCNQ3	NTNG1	SERTAD1	TRIM15
BEND5	CYB5R2	GSG1	KCNS3	OCIAD2	SLAMF9	TRIM36
BEX5	DGKG	GST01	KHDRBS3	OXCT1	SLC40A1	TSPAN13
BTG4	DHRS9	GSTP1	KIAA0746	PAEP	SLC43A3	TSPAN8
C13orf38	DUSP13	GULP1	KIFAP3	PARVA	**SMARCA4**	TUBA3C
C15orf52	DUSP4	HBE1	KLF8	PCP4L1	SNORD123	TWF1
C19orf33	**DUSP6**	HBG1	KRT18P40	PCSK9	SOD3	UBD
C1orf105	DYNLT3	HCG26	LAMA3	PDE4B	SPANXA1	ULBP2
C1orf225	EDNRA	HCLS1	LOC1001309	PDK1	SPANXB2	WIPF1
C1orf54	EGR1	HCN1	LOC1001331	PHLDA2	SPANXD	ZNF503
C21orf99	EGR4	HCP5	LOC145757	PITX2	SPHK1	
C2orf78	**EHF**	HEPH	LOC344887	PKIA	SPINK1	
C4orf26	ELOVL6	HLA-B	LOC554202	PLAT	SPINK5L3	
C6orf115	ENTPD3	HLA-C	LOC654433	POLB	SPRY2	
C6orf141	EPHA1	HLA-E	LOC728148	PON3	SRPX	

NOTE: We identified 275 genes that showed reduced expression in both Brg1i.1 and Brg1i.2 cell lines. Bolded genes were selected for further study.

avoid overdigestion (27). H358 Control, Brg1i.2, and Brg1i.1 pooled cell lines were harvested at 60% to 80% confluence. Cells were then removed by treatment with trypsin-ethylenediaminetetraacetic acid (EDTA) and resuspended in 1 mL reticulocyte-specific buffer [10 mmol/L Tris-HCl (pH 7.4), 10 mmol/L NaCl, 3 mmol/L $MgCl_2$] and placed on ice for 10 minutes, followed by addition of 0.1 mL 10% NP-40 detergent for 30 minutes. After two washes with reticulocyte-specific buffer, nuclei were stored at —80°C. For MNase digestion, extracts were resuspended in 0.2 mL 1× MNase reaction buffer [10 mmol/L Tris-HCl (pH 7.5), 5 mmol/L $MgCl_2$, 5 mmol/L $CaCl_2$, 0.1 mmol/L phenylmethylsulfonylfluoride, 0.5 mmol/L dithiothreitol), aliquoted into 0.5 mL samples with an OD_{260} of 0.2 and treated with 10 U of MNase (Affymetrix) for 10 minutes. MNase was inactivated with the addition of 10 mmol/L EDTA and ethylene glycol-bis(2-aminoethylether)-N,N,N′,N′-tetraacetic acid (EGTA). All samples were then treated with RNase A and Proteinase K followed by DNA isolation by phenol–chloroform extraction and ethanol precipitation. DNA was resuspended in 10 μL 0.1×TE and run on a 2% agarose gel to separate nucleosomes. The mononucleosome band was cut from the gel and purified with the Qiagen Gel Extraction Kit (Qiagen). The manufacturer's protocol was followed with the exception that six volumes of QG (Qiagen, catalog no. 19063) were used to dissolve the gel, two gel volumes of isopropanol were used, and DNA was eluted with 30 μL elution buffer.

Solexa Library Preparation and Illumina sequencing

Libraries were created following the manufacturer's specifications (Illumina). Library preparation included blunt ending of DNA, addition of a polyA-overhang, adapter ligation (Illumina), two times SPRI beads clean up, PCR amplification with PfuUltra II Fusion HS DNA Polymerase (Stratagene), and size selection from a 2% agarose gel. After library generation, paired-end sequencing was performed (Illumina HiSeq2000; UNC Chapel Hill High Throughput Sequencing Facility).

MNase-seq analysis

Paired-end reads were aligned to the reference human genome (hg19) using Bowtie v1.0.0 (28), and samtools v0.1.19 (29) was used for necessary file conversions. DANPOS (30) was used to predict size and positions of nucleosomes. DANPOS default parameters were used with the exceptions of 50 base pair smoothing, single base pair resolution, and a minimum nucleosome size of 146 base pairs. DANPOS was also used to predict nucleosomes and calculate positional conservation scores. BEDTools v2.17.0 (31) and R v2.15.1 were used to extract genomic regions and for subsequent analyses using default parameters. Local trends in MNase signal were removed using the kernel smoothing function in R with a bandwidth of 250 bp. Heatmaps were generated using MATLAB v2012b. UCSC genome browser (32) was used to visualize gene and signal tracks. Transcriptional starts sites (TSS) used were defined by RefSeq, whereas CCCTC-Binding Factor (Zinc Finger Protein) (CTCF) sites were predicted by MotifMap (33).

Results

Reduced BRG1 expression in NSCLC cells induces *in vitro* and *in vivo* growth changes

To determine the effects of BRG1 loss on NSCLC development, we generated BRG1 knockdown clonal cell lines derived from the human NSCLC H358 cell line (hereafter referred to as "NSCLC cells") that expresses a wild-type BRG1 protein (5). We used two different shRNAs (Brg1i.1 and Brg1i.2) to control for possible off-target effects. In general, the Brg1i.2 shRNA proved more efficient at reducing BRG1 mRNA and protein levels than the Brg1i.1 shRNA. Therefore, to control for clonal variation, we generated pools of at least four clonally derived cell lines from each BRG1 shRNA or the vector control, referred to as "Control" (Supplementary Fig. S1). Cells with reduced BRG1 expression exhibited a consistent change in cellular morphology from a tightly packed and cuboidal appearance to an elongated morphology with distinct cellular borders (Fig. 1A).

We next examined whether BRG1 loss altered the tumorigenic potential of NSCLC cells *in vivo*. Parental, Control, and Brg1i.1 cell lines were orthotopically inoculated into the lungs of athymic nude mice. Reduced expression of BRG1 led to decreased survival (mean survival = 37.5 days) compared with either the parental cell line (mean survival = 110 days, $P < 0.05$) or the control (mean survival = 100 days, $P < 0.018$; Fig. 1B). The reduced survival correlated with the appearance of larger tumors within the lung and mediastinum in mice with the Brg1i.1 cells compared with small tumors limited to the lungs

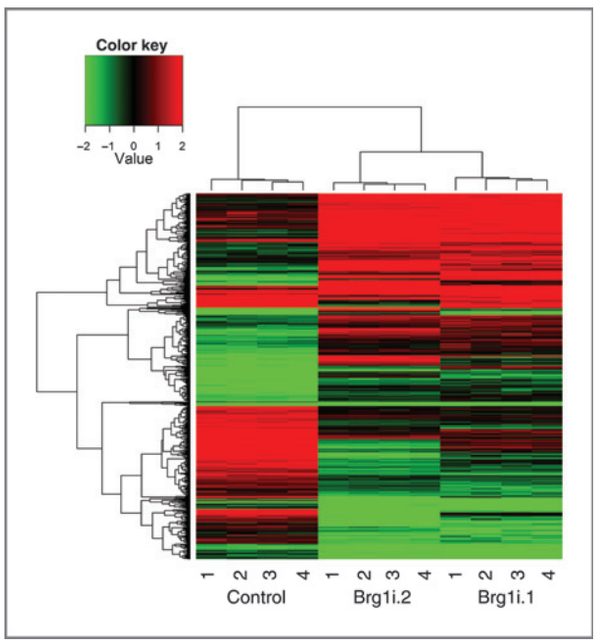

Figure 2. Gene expression changes in response to BRG1 silencing. Heatmap visualization of gene expression values for 591 differentially expressed genes, in which rows are genes and columns are cell line replicates. Expression levels are indicated by the shading in the heatmap. BRG1 knockdown cell lines (Brg1i.1 and Brg1i.2) exhibit highly concordant expression patterns that differ markedly from those seen in control cell lines (Control). Dendrograms show the results of hierarchical clustering of genes and cell line replicates, and all replicates cluster together.

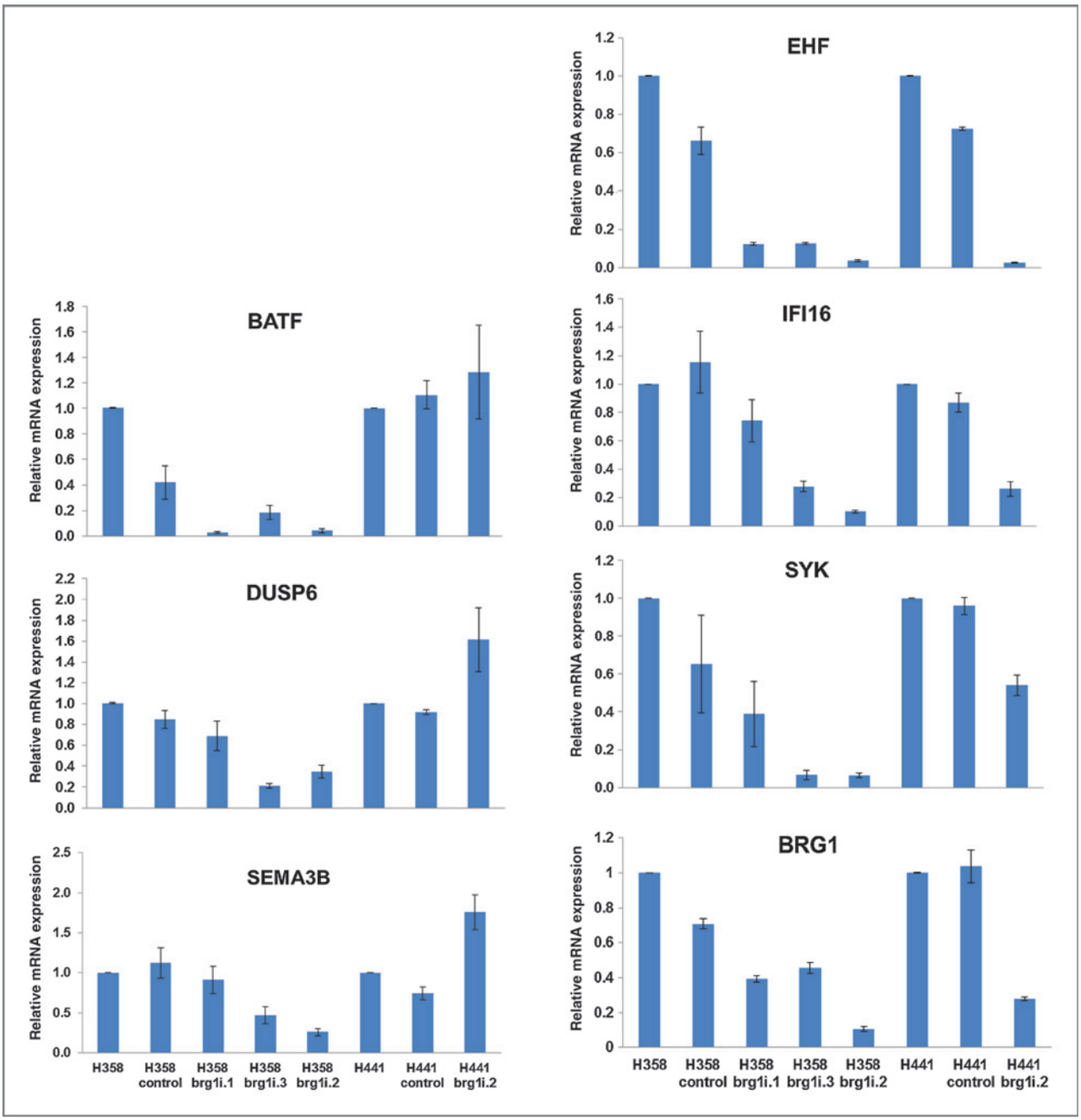

Figure 3. Characterization of BRG1 target gene expression in BRG1 knockdown cell lines. mRNA expression of *BRG1* and six putative target genes in BRG1 knockdown H358 and H441 cell lines was assessed by qRT-PCR as described in Materials and Methods. The mRNA level of each gene was by qPCR and normalized for β-actin expression. Values are the mean of at least two replicates of two independent experiments; bars, ± SD.

of the animals with Control cells (Fig. 1C). Therefore, knockdown of BRG1 expression resulted in dramatic changes in the tumorigenic potential of NSCLC cells.

BRG1 reduction causes specific changes in gene expression

We next asked how BRG1 loss might lead to the observed *in vitro* and *in vivo* changes. Because of the SWI/SNF complex's role in regulating gene transcription, we determined the effects of reduced BRG1 protein levels on gene expression. We identified genes that were differentially expressed between either the Brg1i.1 or Brg1i.2 cell lines relative to parental cells (median FDR < 0.001; Supplementary Table S1—genes altered by BRG1 KD). Consistent with more efficient BRG1 silencing, a greater number of genes demonstrated differential expression in the Brg1i.2 cells when compared with the parental cells (2,050 downregulated and 2,251 upregulated) than the H358 Brg1i.1 cells (363 downregulated and 454 upregulated).

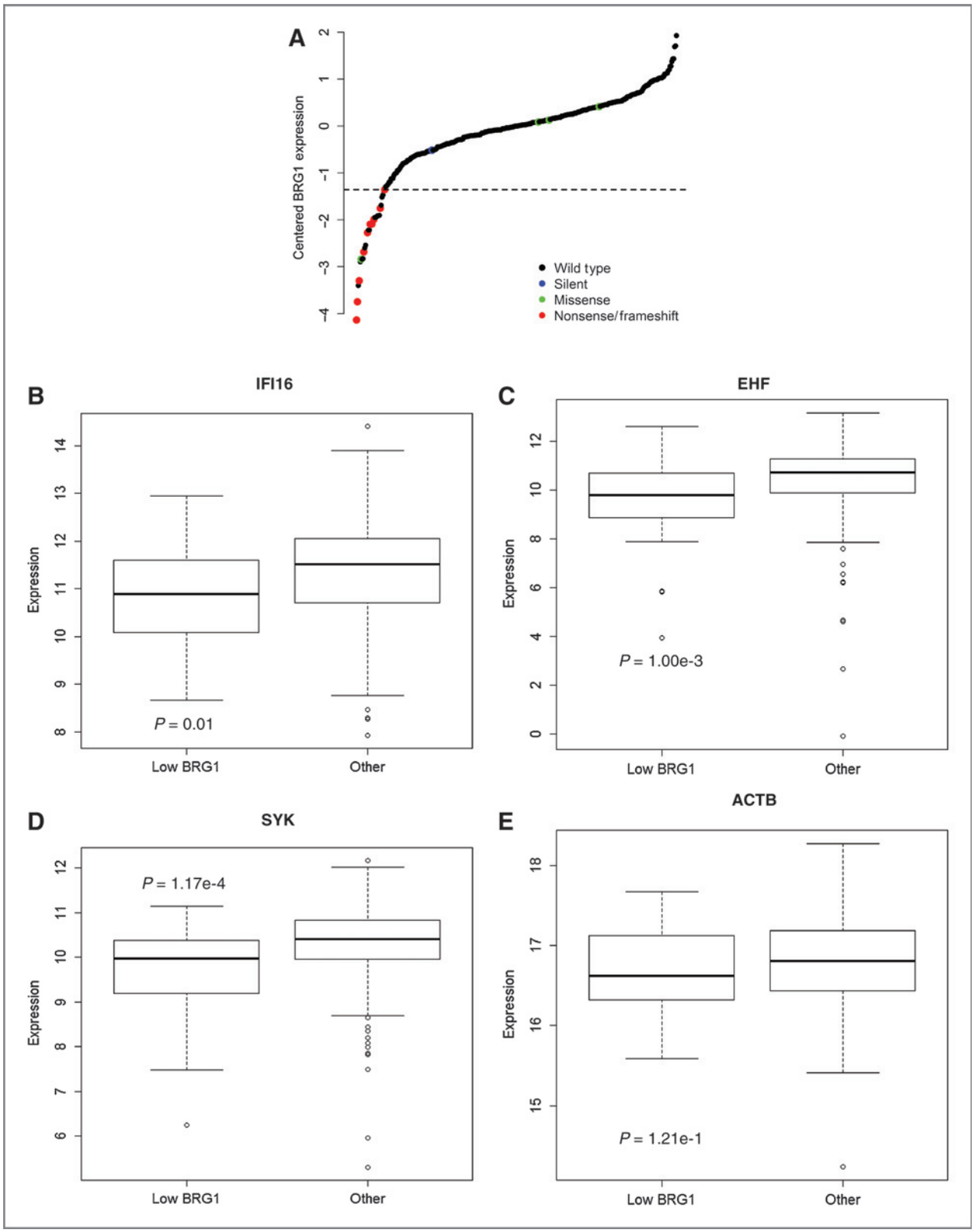

Figure 4. Expression of BRG1 target genes in lung adenocarcinoma. A, median-centered expression values of wild-type and mutant BRG1 in the TCGA lung adenocarcinoma cohort are plotted. Color coding indicates mutation status, and samples below the dashed line are classified as having low BRG1 expression. B–E, boxplots comparing expression values of BRG1 target genes for samples with low BRG1 expression versus other in the TCGA lung adenocarcinoma cohort. Two-sided Wilcoxon rank sum *P* values are shown.

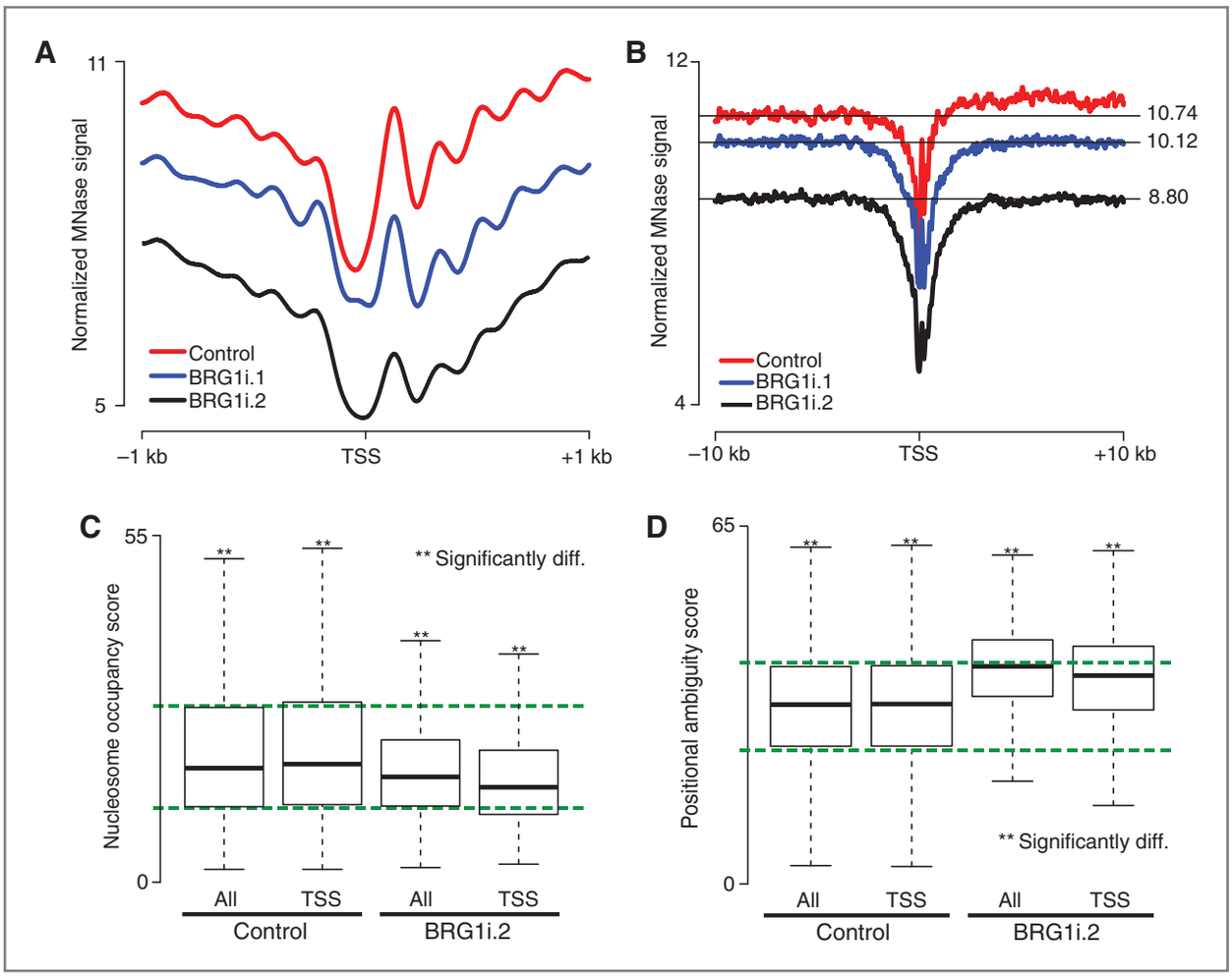

Figure 5. BRG1 loss results in variation in nucleosome occupancy and positioning. MNase signal was normalized to a global average across the three experimental conditions. Signal ±1 kb (A) and ±10 kb (B) were plotted around the TSS at single base pair resolution (red, Control; blue, Brg1i.1; black, Brg1i.2). Nucleosome occupancy scores (C) and positional ambiguity scores (D) were assigned for all predicted nucleosomes in control ($n = 9{,}587{,}862$) and Brg1i.2 ($n = 10{,}344{,}643$) cells (All) or for those predicted to be ±3 kb from TSS in control ($n = 498{,}437$) and Brg1i.2 ($n = 470{,}542$) cells (TSS). Green lines mark the first and third quartile boundaries for all nucleosome in control cells. A two-sided Wilcoxon rank sum test was used to determine significance; **, $P < 10^{-7}$. The center line of each box indicates the median value. Outliers not shown.

We identified 591 genes that were differentially expressed in both BRG1 knockdown cell lines—275 downregulated genes (Table 1) and 316 upregulated genes (Supplementary Table S1—consensus genes). Hierarchical clustering showed highly concordant gene expression patterns among the replicates as well as consistent alterations in gene expression between the each of the two BRG1 knockdown cell lines relative to control cells (Fig. 2). Our previous study had correlated BRG1 loss with reduced expression of genes frequently downregulated during NSCLC development (15), therefore we focused on downregulated genes after BRG1 knockdown in this current study.

Validation of novel targets associated with BRG1 loss

We examined the 275 genes that showed decreased expression in both BRG1 knockdown cell lines for candidates previously associated with cancer development (Table 1). These putative targets included many genes in signaling pathways associated with tumor development, including inflammation (*IL1B*, *IL23A*, *IFI16*, and *FAS*), cell invasion (*ICAM1*, *ICAM2*, and *MMP7*) and cell proliferation (*AREG*, *BATF*, and *SYK*). We additionally identified three genes with reduced expression that had been previously associated with the development of lung and other cancers: *DUSP6*, *EHF*, and *SEMA3B*. *DUSP6* (*MKP3*) is a dual-specificity phosphatase that regulates MAPK signaling through inactivation of ERK2 (34, 35), and recent studies have demonstrated decreased *DUSP6* expression in adenocarcinomas of the lung (36, 37). *EHF* (*ESE-3*) is a member of the ETS transcription factor family that has been implicated as a tumor suppressor for prostate cancer as well as a regulator of inflammation in airway epithelium (38, 39). *SEMA3B* codes for a secreted member of the semaphorin/collapsin family (40). The protein plays a critical role in the guidance of growth cones during neuronal development and has been implicated as a tumor-suppressor gene for NSCLC (40–42).

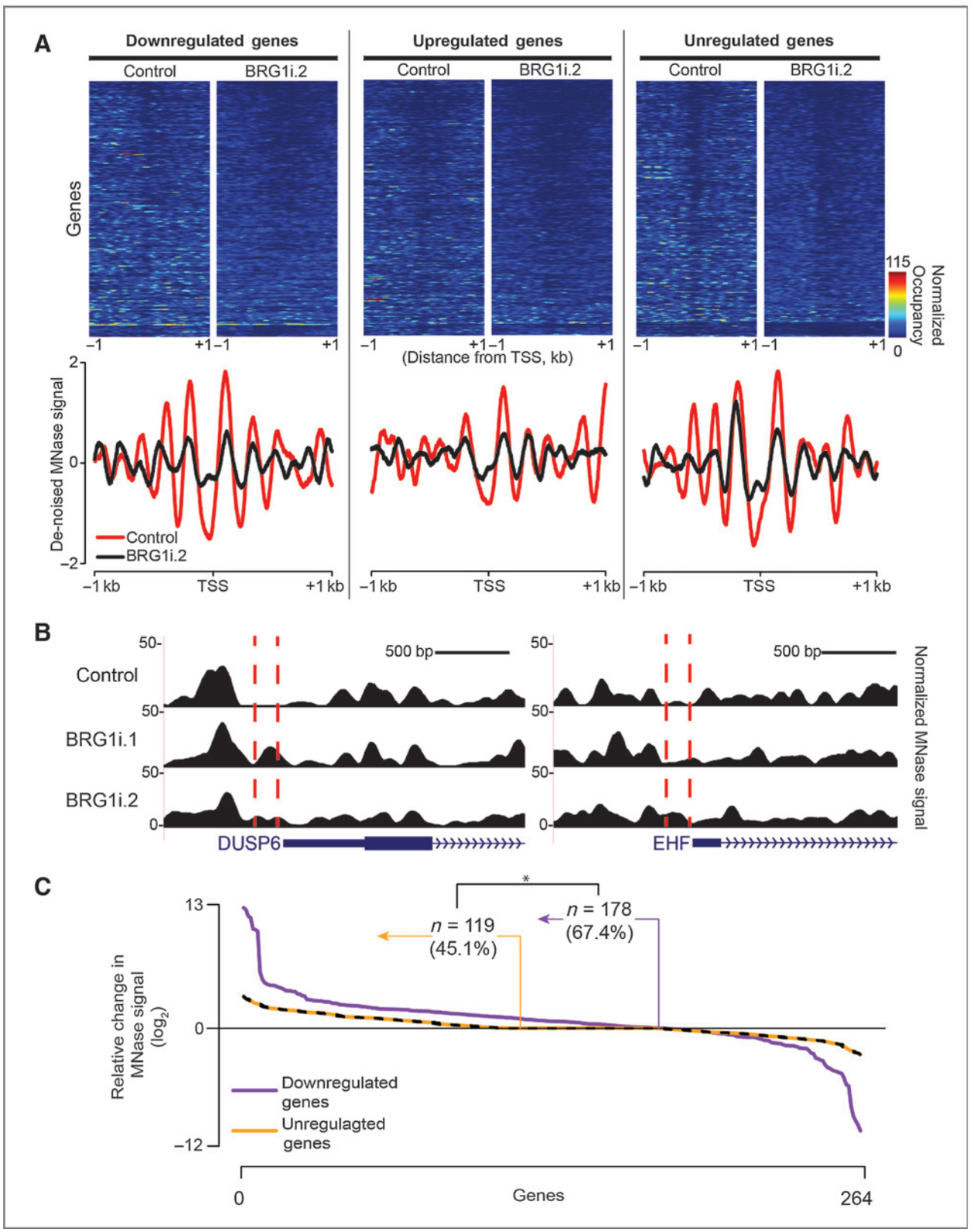

Figure 6. Nucleosomes reposition into the NDR with BRG1 loss. A, heatmaps show normalized nucleosome signal ±1 kb of surrounding RefSeq TSS of downregulated, upregulated, and expression-matched unregulated genes. Each row reflects one gene. Line plots show the kernel smoothed average normalized MNase signal at single base pair resolution for all regions depicted in the heatmap (red, Control; black, Brg1i.2). (*Continued on the following page.*)

We next validated the gene expression differences of six representative genes by qPCR in the BRG1-deficient cell lines as well as a third BRG1-silenced cell line (Brg1i.3; Fig. 3). Reduced levels of mRNA for these genes generally correlated with the degree of BRG1 loss (Fig. 3). We then determined if BRG1 knockdown in a second NSCLC cell line would cause similar changes. We generated a BRG1-deficient H441 cell line using the Brg1i.2 shRNA as well as a nontargeting shRNA Control cell line (Supplementary Fig. S1B). Similar to the H358 Brg1i cell lines, the H441 Brg1i.2 cells show a consistent change in cellular morphology (Supplementary Fig. S1C). A gene expression analysis of our six putative target genes showed reduced expression of three genes with no change or increased expression of the remaining genes (Supplementary Fig. S3). To further validate the remaining target genes, we compared RNA-seq expression data from nine NSCLC cell lines with wild-type BRG1 genes with six cell lines with documented BRG1 truncating/nonsense mutations (5). Using an FDR of 0.025, we confirmed that lower *EHF, IFI16*, and *SYK* expression correlated with BRG1 loss (Supplementary Table S2). Therefore, we identified three candidate genes whose expression decreases in the presence of reduced BRG1 expression.

Target gene expression correlates with BRG1 expression in NSCLC primary tumors

We then asked whether these putative target genes demonstrate similar expression changes in primary human tumors based on BRG1 status. Using the recently released TCGA data for human adenocarcinomas of the lung, we assessed whether *BRG1* gene expression correlated with *BRG1* mutational status. *BRG1* nonsense and frameshift mutations that should lead to truncated or absent protein showed reduced expression of *BRG1* mRNA (Fig. 4A). In contrast, tumors with missense mutations in *BRG1* did not exhibit an obvious change in mRNA expression compared with wild-type *BRG1* tumors (Fig. 4A). On the basis of these observations, we divided the dataset into tumors with either high or low *BRG1* expression. We then asked whether expression of our BRG1 target genes correlated with *BRG1* expression. *EHF, IFI16,* and *SYK* showed a statistically significant association with *BRG1* expression ($P \leq 0.01$, one-sided Wilcoxon rank sum test, Fig. 4B–D). In contrast, we did not observe a statistically significant association for *ACTB* expression ($P = 0.121$, Fig. 4E). Therefore, for these putative downstream targets, expression changes resulting from BRG1 loss in cell lines were similar to those seen in primary tumors.

BRG1 loss alters nucleosome positioning and occupancy

Given the role of SWI/SNF in active chromatin remodeling, we examined nucleosomal differences associated with BRG1 loss. By virtue of its ability to cleave internucleosomal linker DNA, MNase analyzed by high-throughput sequencing (MNase-seq) offers the ability to compare multiple features of nucleosomes. MNase-seq data from control cells and the two BRG1-silenced cell lines were processed to generate normalized signal tracks (DANPOS; ref. 30). Local peaks in MNase signal indicate the presence of nucleosomes and their position, whereas the signal magnitude indicates relative occupancy. Occupancy in this context refers to the fraction of chromatin that is nucleosomal at a specific position among the population of cells being assayed.

We first examined averaged signal around all TSSs. We observed a decrease in overall signal in the −1- to +1-kb region surrounding the TSS (Fig. 5A). This difference was associated with the degree of BRG1 knockdown and indicates that, in aggregate, fewer nucleosomes occupy these regions of chromatin. In all samples, we observed three well-positioned nucleosomes preceding and five nucleosomes following the TSS (designated as —3 to +5). BRG1 knockdown did not alter the position of nucleosomes around the TSS; rather it resulted in signal attenuation that correlated with BRG1 expression levels. An even broader region of well-defined nucleosomes was also observed around CTCF sites (Supplementary Fig. S2A). In contrast to the TSS, relative peak signal attenuation was not observed between samples, although overall signal was diminished, similar to the TSS. We then examined signal further from the TSS and noted that aggregate signal was greater within the gene body compared with upstream regions (Fig. 5B). This polarity was lost when BRG1 was knocked down (Fig. 5B). To correlate BRG1 chromatin interaction with variation in MNase signal after BRG1 knockdown, we overlaid differential MNase signal with publicly available BRG1 ChIP-seq signal around the TSS (43). BRG1 ChIP signal is greatest at the region of maximal MNase signal change (Supplementary Fig. S2B). Together, these data suggest that BRG1 plays an influential role in maintenance of nucleosomes at the TSS.

Individual nucleosomes were then computationally predicted and assigned occupancy and positional ambiguity scores. These scores were then compared between the control and BRG1 knockdown cells. Occupancy scores for individual nucleosomes were diminished genome-wide when BRG1 was knocked down (Fig. 5C; Supplementary Fig. S2C). Variation in occupancy was also observed at TSS-proximal (± 3 kb) nucleosomes. As anticipated, nucleosomes near the TSS demonstrated higher occupancy scores compared with nucleosomes genome-wide. However, BRG1 silencing resulted in TSS-proximal nucleosomes with occupancy lower than nucleosomes genome-wide. These data indicate that nucleosomes with the highest occupancy scores demonstrate the greatest change in the absence of BRG1 with the TSS-proximal nucleosomes being most affected. We also scored nucleosomes based on predicted positional ambiguity. Ambiguity score measures signal

(*Continued.*) B, UCSC genome browser tracks showing window-smoothed, normalized MNase signal around individual TSS. Red lines, region used to define the NDR. C, signal difference between the —1 nucleosome and the NDR (—1nuc — NDR) for each gene in the set (purple, downregulated genes; orange, unregulated genes). The log-transformed ratio of signal difference between control and Brg1i.2 was plotted for each gene $\log_2\left(\frac{(-1nuc-NDR)_{control}}{(-1nuc-NDR)_{BRG1i.2}}\right)$. The unregulated gene set was sampled to match the number of downregulated genes 1,000 times. The average value for each position from the sampling was plotted, and black dashed lines indicate the SD from this sampling. Significance between the downregulated and unregulated gene sets was determined using a Kolmogorov–Smirnov test.

characteristics indicative of variable positioning among the cell population. A higher score indicates increased ambiguity. The loss of BRG1 was associated with increased positional ambiguity overall (Fig. 5D and Supplementary Fig. S2B). However, in contrast to occupancy, TSS-proximal nucleosomes demonstrated less change in positional ambiguity when compared with nucleosomes genome-wide. These data suggest that relative to nucleosomes genome-wide, BRG1 plays a greater role in maintaining occupancy at the TSS but relatively less of a role in maintaining the positioning of these nucleosomes. This is consistent with the role of factors such as RNA polymerase in the maintenance of nucleosome positioning around the TSS (44).

We then examined MNase signal around the TSS of those genes differentially expressed after BRG1 knockdown. We also compared signals around the TSS for a set of genes that were expression-level matched to the downregulated genes but without altered expression after BRG1 knockdown (designated as unregulated genes; Supplementary Table S1). Because, as a group, RNA levels were higher for the downregulated gene set, expression-level matching was performed to control for the effect of gene expression on MNase signal. We observed decreased signal around TSS in BRG1-silenced cells (Fig. 6A, top and Supplementary Fig. S3). This difference was most clearly observed downstream of the TSS. To better characterize differences between samples, MNase signal was denoised to remove the effect of general signal depletion around the TSS (Fig. 6A, bottom and Supplementary Fig. S4). Signal peaks corresponding to nucleosomes were diminished, most notably around the downregulated genes, affecting the −2 to +2 nucleosomes. In the absence of BRG1, signal at the nucleosome depleted region (NDR) was increased. This effect was also evident, albeit to a lesser degree, when all genes were examined (Supplementary Fig. S4A). This effect was observed when we similarly analyzed a previously published dataset from BRG1 knockout murine embryonic fibroblasts (Supplementary Fig. S4B; ref. 45). Signal at the TSS of a subset of downregulated genes exemplifies this effect and suggests a correlation with the level of BRG1 expression (Fig. 6B and Supplementary Fig. S5).

To further explore this effect, we calculated the ratio of differences in MNase signal between the −1 nucleosome and the NDR for Control and Brg1i.2 samples at each gene in the downregulated and unregulated gene sets. This analysis was performed in the absence of kernel smoothing to eliminate potential effects associated with this correction technique. Loss of BRG1 resulted in a greater MNase signal change for the downregulated genes compared with the unregulated genes. The predominant difference for the downregulated genes (compared with the matched unregulated genes) reflected a decreased signal variation between the −1 nucleosome position and NDR ($P < 0.01$ based on permutation of a 1,300-gene class of matched unregulated genes; Fig. 6C). Together, these data support that loss of BRG1 is associated with increased relative nucleosome occupancy at the NDR, suggesting that BRG1 may cooperate with RNA Pol II in the eviction and maintenance of nucleosomes around the TSS.

Discussion

Five to 20% of NSCLCs contain reduced or absent SWI/SNF complex activity through mutations in BRG1 and/or BRM (3, 6, 12), and 10% to 20% of NSCLCs have also been found to have mutations in multiple members of the SWI/SNF complex (3–7, 13, 46–49), such as *ARID1A*, *ARID1B*, and *PBRM1*. How loss of components of the SWI/SNF contributes to oncogenesis remains unclear. Here, we show that loss of BRG1 alters chromatin, especially around the TSS of genes. Our findings are consistent with previous studies showing that BRG1 loss affects nucleosome positioning during differentiation of hematopoietic stem cells and in mouse fibroblasts (45, 50). Moreover, our data indicate a critical role for BRG1 to maintain nucleosome positioning and occupancy around the TSS, particularly at the NDR and in gene bodies, and suggest a role for nucleosome positioning in gene expression.

We also find that silencing of BRM, the mutually exclusive SWI/SNF ATPase, in NSCLC cells does not result in reduced expression of the same set of genes as BRG1 (unpublished observation), suggesting BRG1- and BRM-containing SWI/SNF complexes act in a nonredundant fashion to regulate gene expression in NSCLC. Our identification of BRG1 downstream targets allows for a comparison of the role of other complex members in gene regulation and nucleosome positioning using techniques described in this report. We acknowledge that not all of the gene expression differences between the parental and BRG1-silenced cells reflect a direct effect of BRG1 loss. These genes may be indirectly regulated by other modes of epigenetic silencing, microRNAs, or aberrant RNA processing. Further studies including characterization of the chromatin structure surrounding the putative target genes will address this issue.

We have identified three BRG1 target genes (*EHF*, *IFI16*, and *SYK*) that show significantly reduced expression in human NSCLC tumors and cell lines that share low BRG1 expression. *SYK* has previously been identified as putative tumor-suppressor gene for NSCLC and suppresses invasive potential in the BRG1-deficient A549 NSCLC cell line (51, 52). IFI16 has also been reported to act as a tumor suppressor but its role in cancer development remains unclear (53–55). However, reduced expression of *EHF* has only been reported for prostate cancer (38, 56). Downregulation of *EHF* may account for some of the morphologic changes observed (Fig. 1A and Supplementary Fig. S1C) as *EHF* has been shown to contribute to differentiation and proliferation of epithelial cells (57), as well as regulating apoptotic signaling, *EZH2* expression, and epithelial-to-mesenchymal transition in prostate cancer stem cells (26, 34, 36).

The current study offers insights that may reveal new strategies for the treatment of patients with BRG1-deficient cancers by revealing key target genes that fuel NSCLC development. Importantly, patients with BRG1-deficient NSCLC may respond differently to evolving chromatin-targeted treatments, as many of our identified target genes also undergo silencing through other mechanisms including promoter DNA methylation and histone deacetylation in BRG1-expressing cells (36, 38, 41, 42). Treatments such as DNA methylation inhibitors or histone deacetylase inhibitors may be ineffective in activating genes that are repressed due to BRG1 loss-

associated chromatin changes. Treatments that target BRG1 loss need to be further investigated. The identification of genes differentially expressed due to BRG1 deficiency may also provide insights into clinical course or treatment response differences for NSCLC. Identifying pathways associated with genes that are silenced in BRG1-deficient tumors may lead to novel therapeutic approaches (2, 58, 59). Murine models for BRG1-induced tumor development may also provide a convenient avenue for testing new treatments (60, 61).

Disclosure of Potential Conflicts of Interest

No potential conflicts of interest were disclosed.

Authors' Contributions

Conception and design: A. Hepperla, I.J. Davis, B. Weissman
Development of methodology: T. Orvis, M.D. Wilkerson, D.N. Hayes, I.J. Davis
Acquisition of data (provided animals, acquired and managed patients, provided facilities, etc.): T. Orvis, S. Song, J. Simon, N. Desai, M.B. Major, D.N. Hayes, B. Weissman
Analysis and interpretation of data (e.g., statistical analysis, biostatistics, computational analysis): T. Orvis, A. Hepperla, V. Walter, S. Song, J. Simon, J. Parker, M.D. Wilkerson, N. Desai, D.N. Hayes, I.J. Davis, B. Weissman
Writing, review, and/or revision of the manuscript: T. Orvis, A. Hepperla, V. Walter, S. Song, J. Simon, M.D. Wilkerson, N. Desai, D.N. Hayes, I.J. Davis, B. Weissman
Administrative, technical, or material support (i.e., reporting or organizing data, constructing databases): T. Orvis, N. Desai, D.N. Hayes, B. Weissman
Study supervision: I.J. Davis, B. Weissman

Acknowledgments

The authors thank UNC LCCC Genomics Core Services, the UNC-LCCC Animal Studies Core Facility, and the UNC Chapel Hill High Throughput Sequencing Facility for outstanding experimental support. They also thank Tim Palpant, Fang Fang, Jason Lieb, and members of the Davis and Lieb laboratories for constructive input.

Grant Support

This study was supported in part by a UNC Lineberger Clinical/Translational Research Award and grants from NCI (CA138841 to B. Weissman; CA166447 to I.J. Davis; 1-DP2-OD007149-01 to M. Major; and P30 CA016086).

The costs of publication of this article were defrayed in part by the payment of page charges. This article must therefore be hereby marked *advertisement* in accordance with 18 U.S.C. Section 1734 solely to indicate this fact.

Received January 13, 2014; revised June 16, 2014; accepted July 3, 2014; published OnlineFirst August 12, 2014.

References

1. Panani AD, Roussos C. Cytogenetic and molecular aspects of lung cancer. Cancer Lett 2006;239:1–9.
2. Sato M, Shames DS, Gazdar AF, Minna JD. A translational view of the molecular pathogenesis of lung cancer. J Thorac Oncol 2007;2:327–43.
3. Fukuoka J, Fujii T, Shih JH, Dracheva T, Meerzaman D, Player A, et al. Chromatin remodeling factors and BRM/BRG1 expression as prognostic indicators in non-small cell lung cancer. Clin Cancer Res 2004;10:4314–24.
4. Medina PP, Carretero J, Fraga MF, Esteller M, Sidransky D, Sanchez-Cespedes M. Genetic and epigenetic screening for gene alterations of the chromatin-remodeling factor, SMARCA4/BRG1, in lung tumors. Genes Chromosomes Cancer 2004;41:170–7.
5. Medina PP, Romero OA, Kohno T, Montuenga LM, Pio R, Yokota J, et al. Frequent BRG1/SMARCA4-inactivating mutations in human lung cancer cell lines. Hum Mutat 2008;29:617–22.
6. Reisman DN, Sciarrotta J, Wang W, Funkhouser WK, Weissman BE. Loss of BRG1/BRM in human lung cancer cell lines and primary lung cancers: correlation with poor prognosis. Cancer Res 2003;63:560–6.
7. Rodriguez-Nieto S, Canada A, Pros E, Pinto AI, Torres-Lanzas J, Lopez-Rios F, et al. Massive parallel DNA pyrosequencing analysis of the tumor suppressor BRG1/SMARCA4 in lung primary tumors. Hum Mutat 2011;32:E1999–2017.
8. Neigeborn L, Carlson M. Genes affecting the regulation of SUC2 gene expression by glucose repression in Saccharomyces cerevisiae. Genetics 1984;108:845–58.
9. Stern M, Jensen R, Herskowitz I. Five SWI genes are required for expression of the HO gene in yeast. J Mol Biol 1984;178:853–68.
10. Cote J, Quinn J, Workman JL, Peterson CL. Stimulation of GAL4 derivative binding to nucleosomal DNA by the yeast SWI/SNF complex. Science 1994;265:53–60.
11. Kingston RE, Narlikar GJ. ATP-dependent remodeling and acetylation as regulators of chromatin fluidity. Genes Dev 1999;13:2339–52.
12. Muchardt C, Yaniv M. ATP-dependent chromatin remodelling: SWI/SNF and Co. are on the job. J Mol Biol 1999;293:187–98.
13. Weissman B, Knudsen KE. Hijacking the chromatin remodeling machinery: impact of SWI/SNF perturbations in cancer. Cancer Res 2009;69:8223–30.
14. Wilson BG, Roberts CW. SWI/SNF nucleosome remodellers and cancer. Nat Rev Cancer 2011;11:481–92.
15. Banine F, Bartlett C, Gunawardena R, Muchardt C, Yaniv M, Knudsen ES, et al. SWI/SNF chromatin-remodeling factors induce changes in DNA methylation to promote transcriptional activation. Cancer Res 2005;65:3542–7.
16. Strobeck MW, DeCristofaro MF, Banine F, Weissman BE, Sherman LS, Knudsen ES. The BRG-1 subunit of the SWI/SNF complex regulates CD44 expression. J Biol Chem 2001;276:9273–8.
17. Xu K, Ma H, McCown TJ, Verma IM, Kafri T. Generation of a stable cell line producing high-titer self-inactivating lentiviral vectors. Mol Ther 2001;3:97–104.
18. Rosson GB, Bartlett C, Reed W, Weissman BE. BRG1 loss in MiaPaCa2 cells induces an altered cellular morphology and disruption in the organization of the actin cytoskeleton. J Cell Physiol 2005;205:286–94.
19. Link KA, Burd CJ, Williams E, Marshall T, Rosson G, Henry E, et al. BAF57 governs androgen receptor action and androgen-dependent proliferation through SWI/SNF. Mol Cell Biol 2005;25:2200–15.
20. Kuwahara Y, Charboneau A, Knudsen ES, Weissman BE. Reexpression of hSNF5 in malignant rhabdoid tumor cell lines causes cell cycle arrest through a p21(CIP1/WAF1)-dependent mechanism. Cancer Res 2010;70:1854–65.
21. Livak KJ, Schmittgen TD. Analysis of relative gene expression data using real-time quantitative PCR and the 2(-Delta Delta C(T)) method. Methods 2001;25:402–8.
22. Ritchie ME, Silver J, Oshlack A, Holmes M, Diyagama D, Holloway A, et al. A comparison of background correction methods for two-colour microarrays. Bioinformatics 2007;23:2700–7.
23. Tusher VG, Tibshirani R, Chu G. Significance analysis of microarrays applied to the ionizing radiation response. Proc Natl Acad Sci U S A 2001;98:5116–21.
24. Wang K, Singh D, Zeng Z, Coleman SJ, Huang Y, Savich GL, et al. MapSplice: accurate mapping of RNA-seq reads for splice junction discovery. Nucleic Acids Res 2010;38:e178.
25. Li B, Dewey C. RSEM: accurate transcript quantification from RNA-Seq data with or without a reference genome. BMC Bioinformatics 2011;12:323.
26. Bullard JH, Purdom E, Hansen KD, Dudoit S. Evaluation of statistical methods for normalization and differential expression in mRNA-Seq experiments. BMC Bioinformatics 2010;11:94.
27. Ercan S, Lubling Y, Segal E, Lieb JD. High nucleosome occupancy is encoded at X-linked gene promoters in C. elegans. Genome Res 2011;21:237–44.

28. Langmead B, Trapnell C, Pop M, Salzberg SL. Ultrafast and memory-efficient alignment of short DNA sequences to the human genome. Genome Biol 2009;10:R25.
29. Li H, Handsaker B, Wysoker A, Fennell T, Ruan J, Homer N, et al. The sequence alignment/map format and SAMtools. Bioinformatics 2009;25:2078–9.
30. Chen K, Xi Y, Pan X, Li Z, Kaestner K, Tyler J, et al. DANPOS: dynamic analysis of nucleosome position and occupancy by sequencing. Genome Res 2013;23:341–51.
31. Lv J, Liu H, Wu Q, Zhang Y. High-throughput computational approaches to analyzing histone modification next-generation sequencing data. Comput Molecular Biol 2012;2.
32. Kent WJ, Sugnet CW, Furey TS, Roskin KM, Pringle TH, Zahler AM, et al. The human genome browser at UCSC. Genome Res 2002;12:996–1006.
33. Daily K, Patel VR, Rigor P, Xie X, Baldi P. MotifMap: integrative genome-wide maps of regulatory motif sites for model species. BMC Bioinformatics 2011;12:495.
34. Muda M, Boschert U, Dickinson R, Martinou JC, Martinou I, Camps M, et al. MKP-3, a novel cytosolic protein-tyrosine phosphatase that exemplifies a new class of mitogen-activated protein kinase phosphatase. J Biol Chem 1996;271:4319–26.
35. Groom LA, Sneddon AA, Alessi DR, Dowd S, Keyse SM. Differential regulation of the MAP, SAP and RK/p38 kinases by Pyst1, a novel cytosolic dual-specificity phosphatase. EMBO J 1996;15:3621–32.
36. Lee H, Kim JM, Huang SM, Park SK, Kim DH, Kim do H, et al. Differential expression of DUSP6 with expression of ERK and Ki-67 in non-small cell lung carcinoma. Pathol Res Pract 2011;207:428–32.
37. Zhang Z, Kobayashi S, Borczuk AC, Leidner RS, Laframboise T, Levine AD, et al. Dual specificity phosphatase 6 (DUSP6) is an ETS-regulated negative feedback mediator of oncogenic ERK signaling in lung cancer cells. Carcinogenesis 2010;31:577–86.
38. Cangemi R, Mensah A, Albertini V, Jain A, Mello-Grand M, Chiorino G, et al. Reduced expression and tumor suppressor function of the ETS transcription factor ESE-3 in prostate cancer. Oncogene 2008;27:2877–85.
39. Wu J, Duan R, Cao H, Field D, Newnham CM, Koehler DR, et al. Regulation of epithelium-specific Ets-like factors ESE-1 and ESE-3 in airway epithelial cells: potential roles in airway inflammation. Cell Res 2008;18:649–63.
40. Shirvan A, Ziv I, Fleminger G, Shina R, He Z, Brudo I, et al. Semaphorins as mediators of neuronal apoptosis. J Neurochem 1999;73:961–71.
41. Tomizawa Y, Sekido Y, Kondo M, Gao B, Yokota J, Roche J, et al. Inhibition of lung cancer cell growth and induction of apoptosis after reexpression of 3p21.3 candidate tumor suppressor gene SEMA3B. Proc Natl Acad Sci U S A 2001;98:13954–9.
42. Tse C, Xiang RH, Bracht T, Naylor SL. Human Semaphorin 3B (SEMA3B) located at chromosome 3p21.3 suppresses tumor formation in an adenocarcinoma cell line. Cancer Res 2002;62:542–6.
43. Euskirchen GM, Auerbach RK, Davidov E, Gianoulis TA, Zhong G, Rozowsky J, et al. Diverse roles and interactions of the SWI/SNF chromatin remodeling complex revealed using global approaches. PLoS Genet 2011;7:e1002008.
44. Weiner A, Hughes A, Yassour M, Rando OJ, Friedman N. High-resolution nucleosome mapping reveals transcription-dependent promoter packaging. Genome Res 2010;20:90–100.
45. Tolstorukov MY, Sansam CG, Lu P, Koellhoffer EC, Helming KC, Alver BH, et al. Swi/Snf chromatin remodeling/tumor suppressor complex establishes nucleosome occupancy at target promoters. Proc Natl Acad Sci U S A 2013;110:10165–70.
46. Hammerman PS, Hayes DN, Wilkerson MD, Schultz N, Bose R, Chu A, et al. Comprehensive genomic characterization of squamous cell lung cancers. Nature 2012;489:519–25.
47. Imielinski M, Berger AH, Hammerman PS, Hernandez B, Pugh TJ, Hodis E, et al. Mapping the hallmarks of lung adenocarcinoma with massively parallel sequencing. Cell 2012;150:1107–20.
48. Kadoch C, Hargreaves DC, Hodges C, Elias L, Ho L, Ranish J, et al. Proteomic and bioinformatic analysis of mammalian SWI/SNF complexes identifies extensive roles in human malignancy. Nat Genet 2013;45:592–601.
49. Cerami E, Gao J, Dogrusoz U, Gross BE, Sumer SO, Aksoy BA, et al. The cBio cancer genomics portal: an open platform for exploring multidimensional cancer genomics data. Cancer Discov 2012;2:401–4.
50. Hu G, Schones DE, Cui K, Ybarra R, Northrup D, Tang Q, et al. Regulation of nucleosome landscape and transcription factor targeting at tissue-specific enhancers by BRG1. Genome Res 2011;21:1650–8.
51. Coopman PJ, Mueller SC. The Syk tyrosine kinase: a new negative regulator in tumor growth and progression. Cancer Lett 2006;241:159–73.
52. Peng CL, Zhang Y, Sun QF, Zhao YP, Hao YT, Zhao XG, et al. Inhibitory effects of syk transfection on lung cancer cell invasion. Asian Pac J Cancer Prev 2013;14:3001–3.
53. Alimirah F, Chen J, Davis FJ, Choubey D. IFI16 in human prostate cancer. Mol Cancer Res 2007;5:251–9.
54. Choubey D, Deka R, Ho SM. Interferon-inducible IFI16 protein in human cancers and autoimmune diseases. Front Biosci 2008;13:598–608.
55. Kondo Y, Nagai K, Nakahata S, Saito Y, Ichikawa T, Suekane A, et al. Overexpression of the DNA sensor proteins, absent in melanoma 2 and interferon-inducible 16, contributes to tumorigenesis of oral squamous cell carcinoma with p53 inactivation. Cancer Sci 2012;103:782–90.
56. Albino D, Longoni N, Curti L, Mello-Grand M, Pinton S, Civenni G, et al. ESE3/EHF controls epithelial cell differentiation and its loss leads to prostate tumors with mesenchymal and stem-like features. Cancer Res 2012;72:2889–900.
57. Seth A, Watson DK. ETS transcription factors and their emerging roles in human cancer. Eur J Cancer 2005;41:2462–78.
58. Yagui-Beltran A, He B, Raz D, Kim J, Jablons DM. Novel therapies targeting signaling pathways in lung cancer. Thorac Surg Clin 2006;16:379–96, vi.
59. Gupta GP, Nguyen DX, Chiang AC, Bos PD, Kim JY, Nadal C, et al. Mediators of vascular remodelling co-opted for sequential steps in lung metastasis. Nature 2007;446:765–70.
60. Bultman SJ, Herschkowitz JI, Godfrey V, Gebuhr TC, Yaniv M, Perou CM, et al. Characterization of mammary tumors from Brg1 heterozygous mice. Oncogene 2008;27:460–8.
61. Glaros S, Cirrincione GM, Palanca A, Metzger D, Reisman D. Targeted knockout of BRG1 potentiates lung cancer development. Cancer Res 2008;68:3689–96.